Oxidation of the *Para*-Tolyl Radical by Molecular Oxygen under Single Collison Conditions - Formation of the *Para*-Toloxy Radical

Aaron M. Thomas, Tao Yang, Beni B. Dangi, Ralf I. Kaiser*

Department of Chemistry, University of Hawai'i at Mānoa, Honolulu HI 96822, United States

Gap-Sue Kim

Dharma College, Dongguk University, 30, Pildong-ro 1-gil, Jung-gu, Seoul 04620, South Korea

Alexander M. Mebel*

Department of Chemistry and Biochemistry, Florida International University, Miami, Florida 33199, United States

ABSTRACT

Crossed molecular beam experiments were performed to elucidate the chemical dynamics of the *para*-tolyl ($CH_3C_6H_4$) radical reaction with molecular oxygen (O_2) at an average collision energy of 35.3 ± 1.4 kJ mol^{-1}. Combined with theoretical calculations, the results show that *para*-tolyl is efficiently oxidized by molecular oxygen to *para*-toloxy ($CH_3C_6H_4O$) plus ground state atomic oxygen via a complex forming, overall exoergic reaction (experimental: - 33 ± 16 kJ mol^{-1}; computational: - 42 ± 8 kJ mol^{-1}). The reaction dynamics are analogous to those observed for the phenyl (C_6H_5) plus molecular oxygen system which suggests the methyl group is a spectator during *para*-tolyl oxidation, and that application of phenyl thermochemistry and reaction rates to *para* substituted aryls is likely a suitable approximation.

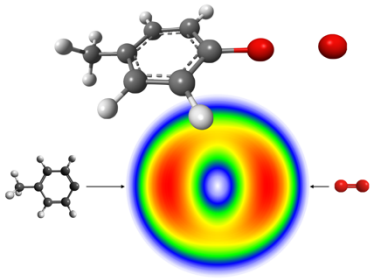

Table of Contents Graphic

Polycyclic aromatic hydrocarbons (PAHs) are rapidly synthesized from reactive remnants produced by the incomplete combustion of fossil fuels,[1–3] a process continuously scrutinized due in part to the carcinogenic and mutagenic properties of aromatic hydrocarbons.[4,5] In recent years, tolyl radials ($CH_3C_6H_4$) (Scheme 1) have been confirmed as central aromatic growth species in the formation of methyl-substituted PAHs such as 1- and 2-methylnapthalene,[6,7] and disubstituted naphthalenes.[8–12] Unlike on Earth, where they are regarded as toxic byproducts of combustion, their large molecular weights and proliferation throughout interstellar space have placed PAHs at the forefront of a multidisciplinary effort to resolve the chemical evolution of the Milky Way. The ubiquity of interstellar PAHs has been inferred by the ultraviolet bump on the interstellar extinction curve (217.5 nm),[13–15] and various features in the diffuse interstellar absorptions bands (0.4 to 1.2 μm)[16,17] and unidentified infrared emission bands (3 to 14 μm).[18–20] Neutral PAHs and their (de)hydrogenated, ionized, and protonated counterparts represent 15-30% of the galactic carbon budget,[21,22] are building blocks for carbonaceous dust grains,[23,24] participate in grain-surface chemistry,[25] and may play a role in the evolution of prebiotic molecules.[26–28] The molecular growth process of (substituted) PAHs involve aromatic radicals such as phenyl (C_6H_5)[29] and tolyl ($CH_3C_6H_4$),[6,7] resonantly stabilized free hydrocarbon radicals like propargyl (C_3H_3),[30] and unsaturated hydrocarbons like acetylene (C_2H_2).[31,32]

During combustion, PAH formation is inhibited by competing oxidation pathways that effectively destroy aromatic radical precursors necessary for rapid PAH growth. Using crossed molecular beams[33–35] and pyrolytic reactors[36] combined with electronic structure calculations, examinations of the simplest aromatic radical, phenyl, with molecular oxygen revealed that at temperatures above 1,000 K, oxidation is highly efficient and is initiated by the formation of a rovibrationally excited phenylperoxy radical intermediate $[C_6H_5OO]^*$ that preferentially

decomposes to the phenoxy radical (C_6H_5O) via O atom loss. Whereas an understanding of the chemical dynamics of the reaction of the phenyl radical with molecular oxygen has begun to emerge recently, beyond computational endeavors[37–39] little is known on the oxidation of the simplest methyl-substituted aromatic radical – tolyl (Scheme 1). Recently, the *o*-tolyl – O_2 system was examined by trapping a distonic *o*-tolyl radical cation in an oxygen bath. *Ortho*-quinone moiety formation via hydroxyl (OH) loss was the only dissociation channel observed, which was also predicted to be the minimum energy pathway by the accompanying (G3SX(MP3)) analysis.[40]

In this Letter, we share the recent findings of a combined experimental and computational study of the gas phase neutral-neutral bimolecular reaction of the *p*-tolyl ($CH_3C_6H_4$) radical with molecular oxygen to form the resonantly stabilized *p*-toloxy radical ($CH_3C_6H_4O$) under single collision conditions. We provide irrefutable evidence that *p*-tolyl radicals are effectively oxidized and thus removed from the pool of available aromatic radicals that would otherwise lead to the formation of methyl-substituted PAHs. C_7H_7 isomers are produced by the combustion of toluene. While conversion to the benzyl radical is thermodynamically preferred, approximately 14% of primary products are tolyl radicals produced by abstraction of toluene's phenylic hydrogen atoms near 900 K.[41,42] Also, tolyl forms competitively with benzyl ($C_6H_5CH_2$) in dicarbon (C_2) reactions with isoprene (C_5H_8),[43] is a pyrolysis product of xylenes (dimethyl-benzenes, $C_6H_4(CH_3)_2$) via methyl-loss (CH_3),[44] and has been predicted as an intermediate (*o*-tolyl) in the thermal decomposition of the benzyl radical.[45] Considering that complex toluene oxidation models still rely on benzene (C_6H_6) and phenyl data to account for the reactivity of the tolyl radicals,[46–48] our investigation provides valuable, experimentally-based insight for future

combustion models that involve the degradation (oxidation) of alkyl-substituted aromatic radicals.

The oxidation of the *p*-tolyl radical was studied under single collision conditions in a crossed molecular beams machine[49,50] by perpendicularly crossing supersonic beams of neat molecular oxygen (O_2; $X^3\Sigma_g^-$) and *p*-tolyl ($CH_3C_6H_4$; X^2A_1)[6] at an average collision energy (E_C) of 35.3 ± 1.4 kJ mol^{-1}. Reactively scattered products were found using a triply differentially pumped quadrupole mass spectrometer preceded by an electron impact ionizer (2 mA, 80 eV). Time-of-flight (TOF) spectra at mass-to-charge ratios (*m/z*) of 123 ($C_7H_7O_2^+$; adduct), 122 ($C_7H_6O_2^+$; atomic hydrogen elimination), 121 ($C_7H_5O_2^+$; molecular hydrogen elimination), 107 ($C_7H_7O^+$; atomic oxygen elimination), and 106 ($C_7H_6O^+$; hydroxyl elimination), were recorded at the center-of-mass (CM) angle of 10.0 ± 0.1˚. A reactive scattering signal was only observed at *m/z* = 107 (Fig. 1), suggesting that the formation of C_7H_7O isomer(s) via atomic oxygen loss is the *only* open channel under our experimental conditions. The corresponding laboratory angular distribution was obtained by integrating the angular-dependent TOF spectra of *m/z* = 107 ($C_7H_7O^+$), recorded in 2.5˚ intervals from 7.25˚ to 24.75˚ (Fig. 2), and reveals a maximum at the CM angle. A non-reactive scattering signal from *p*-tolyl beam constituents could be observed at 7.25˚; following a control experiment which substituted the reactive O_2 beam for a non-reactive N_2 beam, the non-reactive signal was subtracted from the TOF spectrum recorded at 7.25˚. To summarize, the laboratory data provide evidence on the formation of C_7H_7O isomer(s) plus atomic oxygen in the reaction of the *p*-tolyl radical with molecular oxygen under single collision conditions.

To obtain information on the scattering dynamics and to identify the product isomer(s) formed, the laboratory data are transformed into the CM reference frame using a forward

convolution routine.[51] This procedure yields CM descriptions of the translational energy ($P(E_T)$) and angular ($T(\theta)$) flux distributions (Fig. 3). The laboratory data could be fit with a single channel leading from the *p*-tolyl ($CH_3C_6H_4$; 91 amu) and molecular oxygen (O_2; 32 amu) reactants to the formation of the C_7H_7O isomer(s) (107 amu) plus atomic oxygen (O; 16 amu). First, the CM translational energy distribution, $P(E_T)$, helps to assign the product isomer(s). For molecules formed without internal excitation, the high energy cutoff, $P(E_{Tmax})$, of 68 ± 16 kJ mol^{-1} represents the sum of the reaction exoergicity and the collision energy. A subtraction of the collision energy reveals that the reaction is exoergic by 33 ± 16 kJ mol^{-1}. This value correlates well within the error bars of the computed exoergicity of 42 ± 8 kJ mol^{-1} to form the *p*-toloxy (*p*-$CH_3C_6H_4O$) radical plus ground state atomic oxygen (O, ^3P_j). Also, $P(E_T)$ peaks close to zero translational energy with a maximum around 10 kJ mol^{-1} indicating a rather loose exit transition state to form *p*-toloxy and atomic oxygen from a decomposing $[C_7H_7O_2]^*$ intermediate. Therefore, the reverse reaction is reasonably characterized by only a small entrance barrier or even by a barrierless long range association. Finally, on average, 32 ± 9 % of the total available energy is channeled into the translational degrees of freedom of the products; this order of magnitude also suggests indirect scattering dynamics. The CM angular distribution, $T(\theta)$, reveals additional information on the reaction dynamics (Fig. 3). Here, the best fit $T(\theta)$ has maxima at 0˚ and 180˚. The forward-backward symmetry and flux exhibiting over all angles indicate indirect scattering dynamics via a long lived $C_7H_7O_2$ complex, whose lifetime is greater than its rotational period. The minimum at 90˚ further implies geometrical constraints on the exit transition state(s) and suggests that the oxygen atom is emitted within the plane of the decomposing complex, nearly perpendicular to the total angular momentum vector.[52]

Having identified *p*-toloxy ($CH_3C_6H_4O$) and atomic oxygen as the products in the gas phase reaction of ground state molecular oxygen and *p*-tolyl radicals under single collision conditions, we now merge these results with computational data to untangle the underlying reaction mechanism(s) (Fig. 4). The computation at the G3(MP2,CC)//B3LYP/6-311++G** level of theory determined that molecular oxygen adds barrierlessly to the radical center of *p*-tolyl to form the *p*-tolylperoxy collision complex [i1] ($CH_3C_6H_4OO$) stabilized by 193 kJ mol^{-1} with respect to the separated reactants. Considering trajectories holding the highest symmetry, molecular oxygen adds at the *p*-tolyl radical site along tolyl's effective C_{2v} axis (CH_3-C1-C4). Intermediate [i1] could then undergo unimolecular decomposition via the cleavage of the oxygen-oxygen bond through a transition state located 146 kJ mol^{-1} above [i1] to a van-der-Waals complex [vdW]. The latter is stabilized by 31 kJ mol^{-1} with respect to the separated products and dissociates to *p*-toloxy ($CH_3C_6H_4O$, X^2A') plus atomic oxygen (O, ^3P_j) in an overall exoergic reaction (-42 ± 8 kJ mol^{-1}). These energetics are similar to the *o*-toloxy channel found on the da Silva et al. surface (-46 ± 8 kJ mol^{-1}).[37] The computational predictions agree very well with our experimental findings of indirect scattering dynamics involving a $C_7H_7O_2$ intermediate and a loose, product-like exit transition state, where O-O bond scission occurs late in the reaction coordinate. The experimental reaction dynamics have been significantly constrained through interpretation of both the $T(\theta)$ and $P(E_T)$ distributions for an isomer-specific assignment of C_7H_7O to be *p*-toloxy (*p*-$CH_3C_6H_4O$). In the transition state, the leaving oxygen atom slightly deviates from the molecular plane with the OOCC dihedral angle being close to 31°. However, in the *p*-$CH_3C_6H_4O$…O van der Waals complex the departing oxygen atom returns into the molecular plane and it remains in the plane along the minimal energy path resulting in the

p-$CH_3C_6H_4O$ plus atomic oxygen products, which is in accord with the experimental observations.

The bimolecular reaction of *p*-tolyl with molecular oxygen forming the *p*-toloxy radical plus ground state atomic oxygen is energetically and dynamically similar to that of the analogous reaction of phenyl (C_6H_5) with molecular oxygen forming the phenoxy radical (C_6H_5O) plus O (^3P_j), as examined experimentally[33–35] and computationally.[53,54] Here, molecular oxygen also adds to the radical center of the phenyl radical forming a phenylperoxy intermediate [C_6H_5OO], which is stabilized by 194 kJ mol^{-1} with respect to the separated reactants. This complex also emitted atomic oxygen via a loose exit transition state located 152 kJ mol^{-1} above [C_6H_5OO] to form a van-der-Waals complex bound by 5 kJ mol^{-1} with respect to the products.[53] The similarity of the title reaction with $C_6H_5 + O_2$ strongly suggests the *para*-substituted methyl group is a spectator in the formation of *p*-toloxy. Thus, the adaptation of phenyl characteristics (e.g. reaction rates and thermochemistry) is likely suitable for *para*- and *meta*-tolyl radicals in combustion settings. *Ortho*-tolyl represents an exception, due in part to unique pathways involving benzylic-hydrogen migration to *ortho*-bound substituents,[37,40] and its relatively short lifetime at combustion relevant temperatures.[55] In real combustion settings, the primary products of the phenyl and tolyl oxidation undergo secondary reactions, and of note here is the thermal decomposition by carbon monoxide (CO) elimination from phenoxy to cyclopentadienyl (C_5H_5),[56–58] and therefore from toloxy to methylcyclopentadienyl (C_6H_7).[59] While phenyl oxidation promotes PAH formation through $C_5H_5 + C_5H_5$ reactions,[60] unlike cyclopentadienyl, methylcyclopentadienyl can isomerize and proceed directly to benzene via atomic hydrogen loss.[61,62] In the phenyl - molecular oxygen system, the phenylperoxy intermediate eliminates carbon dioxide (CO_2) to form cyclopentadienyl, which overall (both via the CO_2 and CO + O

pathways) accounts for up to 30% of products at 1,000 K.[36] As previously discussed, the methyl group does not participate in the initial addition of molecular oxygen to *p*-tolyl, and thus carbon monoxide elimination from *p*-toloxy and carbon dioxide elimination from *p*-methylphenylperoxy to methylcyclopentadienyl are also expected with similar energetics and branching ratios in comparable environments. In summary, *p*-tolyl is oxidized by molecular oxygen to form *p*-toloxy plus ground state atomic oxygen in a complex forming, exoergic reaction (experiment: - 33 ± 16 kJ mol^{-1}; computation: - 42 ± 8 kJ mol^{-1}). These results contribute to the growing discussion surrounding the reactivity of tolyl and to the oxidation of molecular growth species of polycyclic aromatic hydrocarbons (PAHs) in combustion systems.

Methods – Experimental: The oxidation of *p*-tolyl was performed in a crossed molecular beams machine at the University of Hawaii, which enables the study of bimolecular reactions in a single collision environment through the combined use of supersonic sources, beam skimmers, and differentially pumped regions to maintain a mean free path larger than 10^2 m in the reaction chamber. Detection is accomplished in the plane of the reactant beams by a triply differentially pumped, liquid-nitrogen cooled detector that employs a variable electron impact ionizer and quadrupole mass filter (1.2 MHz),[63] and a single particle counter which consists of an aluminum-coated stainless steel target (-22.5 kV), and a scintillator mounted atop a photomultiplier tube (-1.35 kV).[64] *Para*-chlorotoluene (*p*-$CH_3C_6H_4Cl$, Aldrich, 97.5%) was purified by multiple freeze (77 K) - pump (< 30 mTorr) - thaw (293 K) cycles before seeding at 0.3% in helium (99.9999%; Gaspro). The helium seeded precursor was introduced to a 5 mm^2 photodissociation region by a piezoelectric pulsed valve,[65] where the halogenated precursor was photolyzed by 193 nm (Coherent Compex 110, 60 Hz, 12 mJ/pulse) to yield *p*-tolyl radicals.[66,67] The *p*-tolyl radical

beam was velocity selected by a 4-slot chopper disk. On axis characterization at *m/z* 45.5 ($C_7H_7^{2+}$) and a 34 eV ionization energy indicate a peak velocity, v_p = 1542 ± 14 m s^{-1}, and speed ratio S = 10.6 ± 1.4 for the *p*-tolyl radicals. It should be noted that previous crossed beam experiments in our group with *m*- and *p*-tolyl radicals verified that the initially formed *m*- and *p*-tolyl radicals do not isomerize.[6,7,9–11,68,69] In the present study, the *p*-tolyl reactant intercepted a neat, perpendicularly crossed, molecular oxygen (O_2: $X^3\Sigma_g^-$) beam characterized by v_p = 776 ± 20 m s^{-1} and S = 17.4 ± 1.0. Reactively scattered products were ionized at 80 eV (2 mA), and sampled throughout the scattering plane. The dynamics and energetics of the product channel were analyzed in the center-of-mass (CM) frame, a transformation accomplished through the iterative use of a forward convolution routine that assumes separability of the differential cross-section $I(u, \theta) = P(u) \times T(\theta)$. The differential cross section (DCS) is calculated from operator defined parameters in the CM frame, and transformed to the observation frame for comparison with the experimental TOFs and laboratory angular distribution. This process is repeated until the best fit of the experimental data is attained.

Theoretical: To optimize geometries of all local minima structures and transition states we used the hybrid density functional B3LYP[70–73] method with the 6-311++G** basis set. The same B3LYP/6-311++G** method was applied to calculate vibrational frequencies and zero-point energy (ZPE) corrections for the reactants, products, and all intermediates and transition states. To refine the final energies we applied a modified G3(MP2,CC)//B3LYP[74,75] composite scheme with single-point energies computed at the G3(MP2,CC) level using B3LYP optimized structures, according to the following formula

$$E_0[G3(MP2,CC)] = E[RCCSD(T)/6\text{-}311G^{**}] + \Delta E_{MP2} + E(ZPE)$$

where ΔE_{MP2} = E[MP2/G3large] – E[MP2/6-311G**] is a basis set correction and E(ZPE) is the zero-point energy computed at the B3LYP/6-311++G** level. The spin-restricted RUHF-RCCSD(T) version of the coupled cluster method was employed. T1 diagnostics were checked during coupled cluster calculations to ensure that wave functions do not possess any multireference character. The calculation scheme represents a modification of the original G3[76] method. All calculations were performed using the GAUSSIAN 09[77] and MOLPRO 2010[78] program packages.

Acknowledgement

This work was supported by the US Department of Energy, Basic Energy Sciences via DE-FG02-03ER15411 and DE-FG02-04ER15570 to the University of Hawaii and Florida International University,

References

(1) Glassman, I. Soot Formation in Combustion Processes. *Twenty-Second Symp. Combust. Combust. Inst.* **1988**, 295–311.

(2) Mansurov, Z. A. Soot Formation in Combustion Processes (Review). *Combust. Explos. Shock Waves* **2005**, *41*, 727–744.

(3) Eaves, N. A.; Dworkin, S. B.; Thomson, M. J. Assessing Relative Contributions of PAHs to Soot Mass by Reversible Heterogeneous Nucleation and Condensation. *Proc. Combust. Inst.* **2016**, DOI: 10.1016/j.proci.2016.06.051.

(4) Majumdar, D.; Rajaram, B.; Meshram, S.; Chalapati Rao, C. V. PAHs in Road Dust: Ubiquity, Fate, and Summary of Available Data. *Crit. Rev. Environ. Sci. Technol.* **2012**, *42*, 1191–1232.

(5) Kim, K.; Jahan, S. A.; Kabir, E.; Brown, R. J. C. A Review of Airborne Polycyclic Aromatic Hydrocarbons (PAHs) and Their Human Health Effects. *Environ. Int.* **2013**, *60*, 71–80.

(6) Parker, D. S. N.; Dangi, B. B.; Kaiser, R. I.; Jamal, A.; Ryazantsev, M. N.; Morokuma, K.; Korte, A.; Sander, W. An Experimental and Theoretical Study on the Formation of 2-Methylnaphthalene ($C_{11}H_{10}$/$C_{11}H_3D_7$) in the Reactions of the Para-Tolyl (C_7H_7) and Para-Tolyl-d7 (C_7D_7) with Vinylacetylene (C_4H_4). *J. Phys. Chem. A* **2014**, *118*, 2709–2718.

(7) Yang, T.; Muzangwa, L.; Kaiser, R. I.; Morokuma, K. A Combined Crossed Molecular Beam and Meta-Tolyl Radical with Vinylacetylene – toward the Formation of Methylnaphthalenes. *Phys. Chem. Chem. Phys.* **2015**, *17*, 21564–21575.

(8) Parker, D. S. N.; Maity, S.; Dangi, B. B.; Kaiser, R. I.; Landera, A.; Mebel, A. M. Understanding the Chemical Dynamics of the Reactions of Dicarbon with 1-Butyne, 2-

Butyne, and 1,2-Butadiene - toward the Formation of Resonantly Stabilized *Free* Radicals. *Phys. Chem. Chem. Phys.* **2014**, *16*, 12150–12163.

(9) Kaiser, R. I.; Dangi, B. B.; Yang, T.; Parker, D. S. N.; Mebel, A. M. Reaction Dynamics of the 4‑Methylphenyl Radical (*p*‑Tolyl) with 1,2-Butadiene (1-Methylallene): Are Methyl Groups Purely Spectators? *J. Phys. Chem. A* **2014**, *118*, 6181–6190.

(10) Parker, D. S. N.; Dangi, B. B.; Kaiser, R. I.; Jamal, A.; Ryazantsev, M.; Morokuma, K. Formation of 6‑Methyl-1,4-Dihydronaphthalene in the Reaction of the *p*‑Tolyl Radical with 1,3-Butadiene Under Single-Collision Conditions. *J. Phys. Chem. A* **2014**, *118*, 12111–12119.

(11) Muzangwa, L. G.; Yang, T.; Parker, D. S. N.; Kaiser, R. I.; Mebel, A. M.; Jamal, A.; Ryazantsev, M.; Morokuma, K. A Crossed Molecular Beam and Ab Initio Study on the Formation of 5- and 6-Methyl-1,4-Dihydronaphthalene ($C_{11}H_{12}$) via the Reaction of Meta-Tolyl (C_7H_7) with 1,3-Butadiene (C_4H_6). *Phys. Chem. Chem. Phys.* **2015**, *17*, 7699–7706.

(12) Wang, H.; Yu, S.; Su, S.; Dai, D.; Yuan, K.; Yang, X. Photodissociation Dynamics of Diacetylene Rydberg States. *J. Phys. Chem. A* **2015**, *119*, 11313–11319.

(13) Duley, W. W. A Plasmon Resonance in Dehydrogenated Coronene ($C_{24}H_x$) and Its Cations and the Origin of the Interstellar Exctinction Band at 217.5 Nanometers. *Astrophys. J. Lett.* **2006**, *639*, L59–L62.

(14) Malloci, G.; Mulas, G.; Cecchi-Pestellini, C.; Joblin, C. Dehydrogenated Polycyclic Aromatic Hydrocarbons and UV Bump. *Astron. Astrophys.* **2008**, *489*, 1183–1187.

(15) Steglich, M.; Jäger, C.; Rouillé, G.; Huisken, F.; Mutschke, H.; Henning, T. Electronic Spectroscopy of Medium-Sized Polycyclic Aromatic Hydrocarbons: Implications for the Carriers of the 2175 Å UV Bump. *Astrophys. J. Lett.* **2010**, *712*, L16-L20.

(16) Herbig, G. H. The Diffuse Interstellar Bands. *Annu. Rev. Astrophys.* **1995**, *33*, 19–73.

(17) Xiang, F.; Liang, S.; Li, A. Diffuse Interstellar Absorption Bands. *Sci. China Ser. G Physics, Mech. Astron.* **2009**, *52*, 489–501.

(18) Allamandola, L. J.; Tielens, A. G. G. M.; Barker, J. R. Polycyclic Aromatic Hydrocarbons and the Unidentified Infrared Emission Bands - Auto Exhaust along the Milky Way. *Astrophys. J.* **1985**, *290*, L25–L28.

(19) Chan, K.-W.; Roellig, T. L.; Onaka, T.; Mizutani, M.; Okumura, K.; Yamamura, I.; Tanabe, T.; Shibai, H.; Nakagawa, T.; Okuda, H. Unidentified Infrared Emission Bands in the Diffuse Interstellar Medium. *Astrophys. J.* **2001**, *546*, 273–278.

(20) Tielens, A. G. G. M. Interstellar Polycyclic Aromatic Hydrocarbon Molecules. *Annu. Rev. Astron. Astrophys.* **2008**, *46*, 289–337.

(21) Allamandola, L. J.; Tielens, A. G. G. M.; Barker, J. R. Interstellar Polycyclic Aromatic Hydrocarbons: The Infrared Emission Bands, the Excitation/Emission Mechanism, and the Astrophysical Implications. *Astrophys. J. Suppl. Ser.* **1989**, *71*, 733–775.

(22) Snow, T. P.; Witt, A. N. The Interstellar Carbon Budget and the Role of Carbon in Dust and Large Molecules. *Science* **1995**, *270*, 1455–1460.

(23) Draine, B. T. Interstellar Dust Grains. *Annu. Rev. Astron. Astrophys.* **2003**, *41*, 241–289.

(24) Cherchneff, I. The Inner Wind of IRC+10216 Revisited: New Exotic Chemistry and Diagnostic for Dust Condensation in Carbon Stars. *Astron. Astrophys.* **2012**, *545*, A12.

(25) Thrower, J. D.; Friis, E. E.; Skov, A. L.; Jørgensen, B.; Hornekær, L. Hydrogenation of PAH Molecules through Interaction with Hydrogenated Carbonaceous Grains. *Phys. Chem. Chem. Phys.* **2014**, *16*, 3381–3387.

(26) Bernstein, M. P.; Sandford, S. A.; Allamandola, L. J.; Gillette, J. S.; Clemett, S. J.; Zare,

R. N. UV Irradiation of Polycyclic Aromatic Hydrocarbons in Ices: Poduction of Alcohols, Quinones, and Ethers. *Science* **1999**, *283*, 1135–1138.

(27) Allamandola, L. J.; Hudgins, D. M. From Interstellar Polycyclic Aromatic Hydrocarbons and Ice to Astrobiology. In *Solid State Astrochemistry*; Pirronello, V., Krelowski, J., Manicò, G., Eds.; Kluwer Academic Publishers: Dordrecht, the Netherlands.; 2003. pp 251–316.

(28) Ehrenfreund, P.; Sephton, M. A. Carbon Molecules in Space: From Astrochemistry to Astrobiology. *Faraday Discuss.* **2006**, *133*, 277–288.

(29) Kaiser, R. I.; Parker, D. S. N.; Mebel, A. M. Reaction Dynamics in Astrochemistry: Low-Temperature Pathways to Polycyclic Aromatic Hydrocarbons in the Interstellar Medium. *Annu. Rev. Phys. Chem.* **2015**, *66*, 43–67.

(30) Jin, H.; Frassoldati, A.; Wang, Y.; Zhang, X.; Zeng, M.; Li, Y.; Qi, F.; Cuoci, A.; Faravelli, T. Kinetic Modeling Study of Benzene and PAH Formation in Laminar Methane Flames. *Combust. Flame* **2015**, *162*, 1692–1711.

(31) Kislov, V. V.; Islamova, N. I.; Kolker, A. M.; Lin, S. H.; Mebel, A. M. Hydrogen Abstraction Acetylene Addition and Diels-Alder Mechanisms of PAH Formation: A Detailed Study Using First Principles Calculations. *J. Chem. Theo. Comput.* **2005**, *1*, 908–924.

(32) Parker, D. S. N.; Kaiser, R. I.; Troy, T. P.; Ahmed, M. Hydrogen Abstraction/Acetylene Addition Revealed. *Angew. Chem. Int. Ed.*. **2014**, *53*, 7740–7744.

(33) Gu, X.; Zhang, F.; Kaiser, R. I. Crossed Beam Reaction of the Phenyl Radical, (C_6H_5, X_2A') with Molecular Oxygen (O_2, $X^3\Sigma_g^-$): Observation of the Phenoxy Radical, (C_6H_5O, X_2A'). *Chem. Phys. Lett.* **2007**, *448*, 7–10.

(34) Albert, D. R.; Davis, H. F. Collision Complex Lifetimes in the Reaction $C_6H_5 + O_2 \rightarrow C_6H_5O + O$. *J. Phys. Chem. Lett.* **2010**, *1*, 1107–1111.

(35) Parker, D. S. N.; Zhang, F.; Kaiser, R. I. Phenoxy Radical (C_6H_5O) Formation under Single Collision Conditions from Reaction of the Phenyl Radical (C_6H_5, X^2A_1) with Molecular Oxygen (O_2, $X^3\Sigma_g^-$): The Final Chapter? *J. Phys. Chem. A* **2011**, *115*, 11515–11518.

(36) Parker, D. S. N.; Kaiser, R. I.; Troy, T. P.; Kostko, O.; Ahmed, M.; Mebel, A. M. Toward the Oxidation of the Phenyl Radical and Prevention of PAH Formation in Combustion Systems. *J. Phys. Chem. A* **2015**, *119*, 7145-7154.

(37) da Silva, G.; Chen, C.-C.; Bozzelli, J. W. Toluene Combustion: Reaction Paths, Thermochemical Properties, and Kinetic Analysis for the Methylphenyl Radical + O_2 Reaction. *J. Phys. Chem. A* **2007**, *111*, 8663–8676.

(38) Sinha, S.; Raj, A.; Alshoaibi, A. S.; Alhassan, S. M.; Chung, S. H. Toluene Destruction in the Claus Process by Sulfur Dioxide: A Reaction Kinetics Study. *Ind. Eng. Chem. Res.* **2014**, *53*, 16293–16308.

(39) Ma, Y.; Su, K.; Zhang, J.; Wang, Y.; Wang, X.; Liu, Y. Hydrogen Abstraction Mechanisms and Reaction Rates of Toluene + NO_3. *J. Mol. Model.* **2015**, *21*, 207.

(40) Prendergast, M. B.; Cooper, P. a; Kirk, B. B.; da Silva, G.; Blanksby, S. J.; Trevitt, A. J. Hydroxyl Radical Formation in the Gas Phase Oxidation of Distonic 2-Methylphenyl Radical Cations. *Phys. Chem. Chem. Phys.* **2013**, *15*, 20577–20584.

(41) Seta, T.; Nakajima, M.; Miyoshi, A. High-Temperature Reactions of OH Radicals with Benzene and Toluene. *J. Phys. Chem. A* **2006**, *110*, 5081–5090.

(42) Bounaceur, R.; Da Costa, I.; Fournet, R.; Billaud, F.; Battin-Leclerc, F. Experimental and

Modeling Study of the Oxidation of Toluene. *Int. J. Chem. Kinet.* **2005**, *37*, 25–49.

(43) Dangi, B. B.; Parker, D. S. N.; Yang, T.; Kaiser, R. I.; Mebel, A. M. Gas-Phase Synthesis of the Benzyl Radical ($C_6H_5CH_2$). *Angew. Chem. Int. Ed.* **2014**, *53*, 4608–4613.

(44) Gail, S.; Dagaut, P. Experimental Kinetic Study of the Oxidation of *p*-Xylene in a JSR and Comprehensive Detailed Chemical Kinetic Modeling. *Combust. Flame* **2005**, *141*, 281–297.

(45) Derudi, M.; Polino, D.; Cavallotti, C. Toluene and Benzyl Decomposition Mechanisms: Elementary Reactions and Kinetic Simulations. *Phys. Chem. Chem. Phys.* **2011**, *13*, 21308–21318.

(46) Yuan, W.; Li, Y.; Dagaut, P.; Yang, J.; Qi, F. Investigation on the Pyrolysis and Oxidation of Toluene over a Wide Range Conditions. I. Flow Reactor Pyrolysis and Jet Stirred Reactor Oxidation. *Combust. Flame* **2015**, *162*, 3–21.

(47) Yuan, W.; Li, Y.; Dagaut, P.; Yang, J.; Qi, F. Investigation on the Pyrolysis and Oxidation of Toluene over a Wide Range Conditions. II. A Comprehensive Kinetic Modeling Study. *Combust. Flame* **2015**, *162*, 22–40.

(48) Ellis, C.; Scott, M. S.; Walker, R. W. Addition of Toluene and Ethylbenzene to Mixtures of H_2 and O_2 at 772 K: Part 2: Formation of Products and Determination of Kinetic Data for H+ Additive and for Other Elementary Reactions Involved. *Combust. Flame* **2003**, *132*, 291–304.

(49) Guo, Y.; Gu, X.; Kawamura, E.; Kaiser, R. I. Design of a Modular and Versatile Interlock System for Ultrahigh Vacuum Machines: A Crossed Molecular Beam Setup as a Case Study. *Rev. Sci. Instrum.* **2006**, *77*, 1–9.

(50) Gu, X.; Guo, Y.; Kawamura, E.; Kaiser, R. I. Characteristics and Diagnostics of an

Ultrahigh Vacuum Compatible Laser Ablation Source for Crossed Molecular Beam Experiments. *J. Vac. Sci. Technol. A* **2006**, *24*, 505-511.

(51) Vernon, M. F. Molecular Beam Scattering, University of California, Berkeley, 1983.

(52) Levine, R. D. *Molecular Reaction Dynamics*; Cambridge University Press: Cambridge,U.K.; 2005.

(53) Tokmakov, I. V.; Kim, G. S.; Kislov, V. V.; Mebel, A. M.; Lin, M. C. The Reaction of Phenyl Radical with Molecular Oxygen: A G2M Study of the Potential Energy Surface. *J. Phys. Chem. A* **2005**, *109*, 6114–6127.

(54) da Silva, G.; Bozzelli, J. W. Variational Analysis of the Phenyl + O and Phenoxy + O Reactions Variational Analysis of the Phenyl + O_2 and Phenoxy + O Reactions. *J. Phys. Chem. A* **2008**, *112*, 3566–3575.

(55) Dames, E.; Wang, H. Isomerization Kinetics of Benzylic and Methylphenyl Type Radicals in Single-Ring Aromatics. *Proc. Combust. Inst.* **2013**, *34*, 307–314.

(56) Lin, C.-Y.; Lin, M. C. Thermal Decomposition of Methyl Phenyl Ether in Shock Waves: The Kinetics of Phenoxy Radical Reactions. *J. Phys. Chem.* **1986**, *90*, 425–431.

(57) Liu, R.; Morokuma, K.; Mebel, A. M.; Lin, M. C.; V, E. U. Ab Initio Study of the Mechanism for the Thermal Decomposition of the Phenoxy Radical. *J. Phys. Chem.* **1996**, *100*, 9314–9322.

(58) Dagaut, P.; Pengloan, G.; Ristori, A. Oxidation, Ignition and Combustion of Toluene: Experimental and Detailed Chemical Kinetic Modeling. *Phys. Chem. Chem. Phys.* **2002**, *4*, 1846–1854.

(59) Emdee, J.; Brezinsky, K.; Glassman, I. High-Temperature Oxidation Mechanisms of M- and P-Xylene. *J. Phys. Chem.* **1991**, *95*, 1626–1635.

(60) Marinov, N. M.; Pitz, W. J.; Westbrook, C. K.; Vincitore, A. M.; Castaldi, M. J.; Senkan, S. M.; Melius, C. F. Aromatic and Polycyclic Aromatic Hydrocarbon Formation in a Laminar Premixed *n*-Butane Flame. *Combust. Flame* **1998**, *114*, 192–213.

(61) Lockyear, J. F.; Fournier, M.; Sims, I. R.; Guillemin, J. C.; Taatjes, C. A.; Osborn, D. L.; Leone, S. R. Formation of Fulvene in the Reaction of C_2H with 1,3-Butadiene. *Int. J. Mass Spectrom.* **2015**, *378*, 232–245.

(62) Jasper, A. W.; Hansen, N. Hydrogen-Assisted Isomerizations of Fulvene to Benzene and of Larger Cyclic Aromatic Hydrocarbons. *Proc. Combust. Inst.* **2013**, *34*, 279–287.

(63) Brink, G. O. Electron Bombardment Molecular Beam Detector. *Rev. Sci. Instrum.* **1966**, *37*, 857–860.

(64) Daly, N. R. Scintillation Type Mass Spectrometer Ion Detector. *Rev. Sci. Instrum.* **1960**, *31*, 264–267.

(65) Proch, D.; Trickl, T. A High-Intensity Multi-Purpose Piezoelectric Pulsed Molecular Beam Source. *Rev. Sci. Instrum.* **1989**, *60*, 713–716.

(66) Lin, M.-F.; Huang, C.-L.; Kislov, V. V.; Mebel, a. M.; Lee, Y. T.; Ni, C.-K. H and CH_3 Eliminations in the Photodissociation of Chlorotoluene. *J. Chem. Phys.* **2003**, *119*, 7701-7704.

(67) Yuan, L. W.; Zhu, J. Y.; Wang, Y. Q.; Wang, L.; Bai, J. L.; He, G. Z. Real-Time Investigation of the Photodissociation Dynamics of *p*-Chlorotoluene and *p*-Dichlorobenzene. *Chem. Phys. Lett.* **2005**, *410*, 352–357.

(68) Dangi, B. B.; Yang, T.; Kaiser, R. I.; Mebel, A. M. Reaction Dynamics of the 4-Methyphenyl Radical ($C_6H_4CH_3$; *p*-Tolyl) with Isoprene (C_5H_8) - Formation of Dimethyldihydronaphthalenes. *Phys. Chem. Chem. Phys.* **2014**, *16*, 16805–16814.

(69) Yang, T.; Muzangwa, L.; Kaiser, R. I.; Jamal, A.; Morokuma, K. A Combined Crossed Molecular Beam and Theoretical Investigation of the Reaction of the Meta-Tolyl Radical with Vinylacetylene – toward the Formation of Methylnaphthalenes. *Phys. Chem. Chem. Phys.* **2015**, *17*, 21564-21575.

(70) Becke, A. D. Density-Functional Thermochemistry. I. The Effect of the Exchange-Only Gradient Correction. *J. Chem. Phys.* **1992**, *96*, 2155–2160.

(71) Becke, A. D. Density-Functional Thermochemistry. II. The Effect of the Perdew–Wang Generalized-Gradient Correlation Correction. *J. Chem. Phys.* **1992**, *97*, 9173.

(72) Becke, A. D. Density-Functional Thermochemistry. III. The Role of Exact Exchange. *J. Chem. Phys.* **1993**, *98*, 5648.

(73) Lee, C.; Yang, W.; Parr, R. G. Development of the Colle-Salvetti Correlation-Energy Formula into a Functional of the Electron Density. *Phys. Rev. B* **1988**, *37*, 785–789.

(74) Baboul, A. G.; Curtiss, L. A.; Redfern, P. C.; Raghavachari, K. Gaussian-3 Theory Using Density Functional Geometries and Zero-Point Energies. *J. Chem. Phys.* **1999**, *110*, 7650–7657.

(75) Curtiss, L. A.; Raghavachari, K.; Redfern, P. C.; Baboul, A. G.; Pople, J. A. Gaussian-3 Theory Using Coupled Cluster Energies. *Chem. Phys. Lett.* **1999**, *314*, 101–107.

(76) Curtiss, L. A.; Raghavach Ari, K.; Redfern, P. C.; Rassolov, V.; Pople, J. A. Gaussian-3 (G3) Theory for Molecules Containing First and Second-Row Atoms. *J. Chem. Phys.* **1998**, *109*, 7764–7776.

(77) Frisch, M. J.; Trucks, G. W.; Schlegel, H. B.; Scuseria, G. E.; Robb, M. A.; Cheeseman, J. R.; Scalmani, G.; Barone, V.; Mennucci, B.; Petersson, G. A.; et al. Gaussian 09, Revision B.01 (Gaussian, Inc., Wallingford CT, 2010).

(78) Werner, H.-J.; Knowles, P. J.; Knizia, G.; Manby, F. R.; Schultze, M.; Celani, P.; Korona, T.; Lindh, R.; Mitrushenkov, A.; Rauhut, G. *MOLPRO*, version 2010.1, A Package of Ab Initio Programs. 2010.

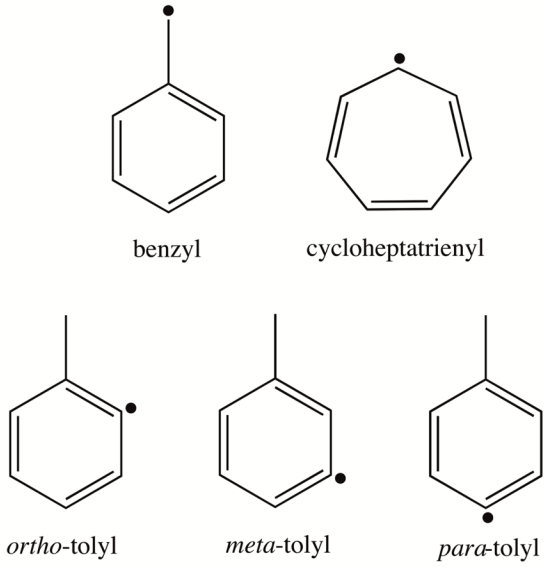

Scheme 1. Structural isomers of the C_7H_7 radical.

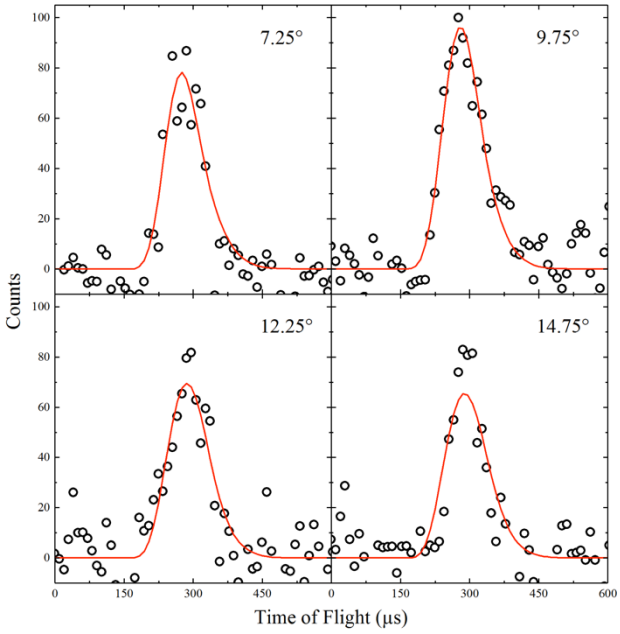

Figure 1. Angularly resolved time-of-flight spectra detected at m/z = 107 ($C_7H_7O^+$) resulting from the reactive scattering of the *p*-tolyl radical (C_7H_7) with molecular oxygen (O_2). Laboratory (observation) angles are indicated for each distribution. Open circles indicate experimentally measured data and red lines the scattering simulation.

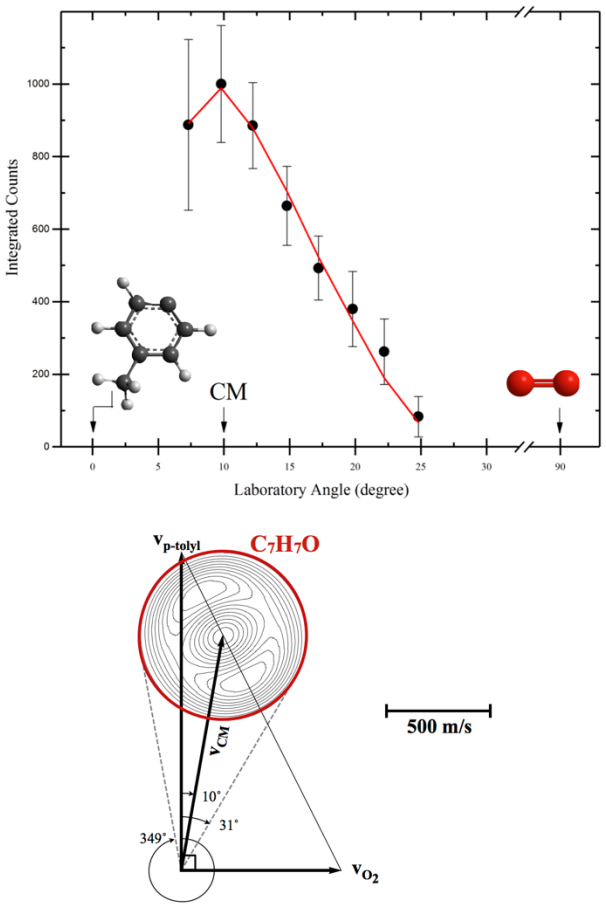

Figure 2. *Top*. Laboratory angular distribution of C_7H_7O derived from the angularly resolved time-of-flight spectra recorded at m/z 107 ($C_7H_7O^+$) from 7.25˚ to 24.75˚. The black dots are experimental data (±1σ), and the red line is the best fit. *Bottom*. Newton diagram for the $CH_3C_6H_4 + O_2 \rightarrow C_7H_7O + O$ reaction. The red circle has radius equal to the maximum CM velocity of C_7H_7O (derived from fit), and is restricted to a 42˚ wedge in the laboratory frame (hashed lines).

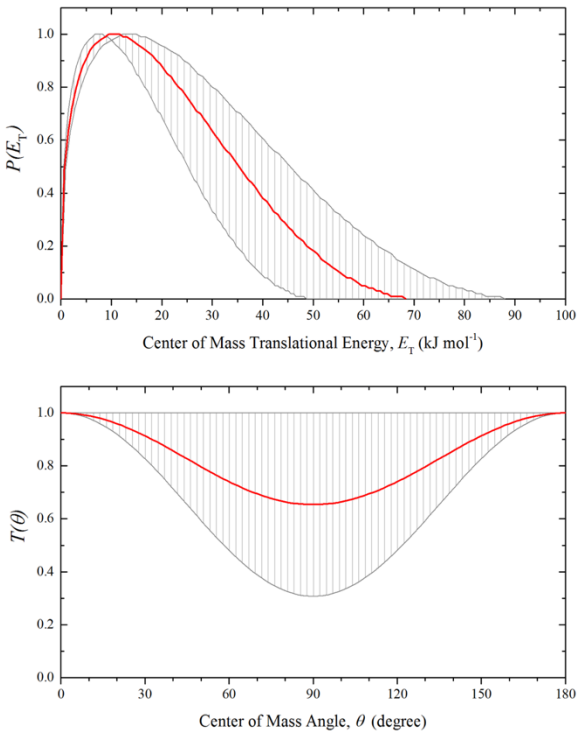

Figure 3. Center-of-mass translational energy (top) and angular (bottom) flux distributions *p*-toloxy radical (C_7H_7O; 107 amu) produced from the *p*-tolyl radical reaction with molecular oxygen. Hatched areas indicate the acceptable upper and lower error limits of the fits. The solid lines define the best fit function.

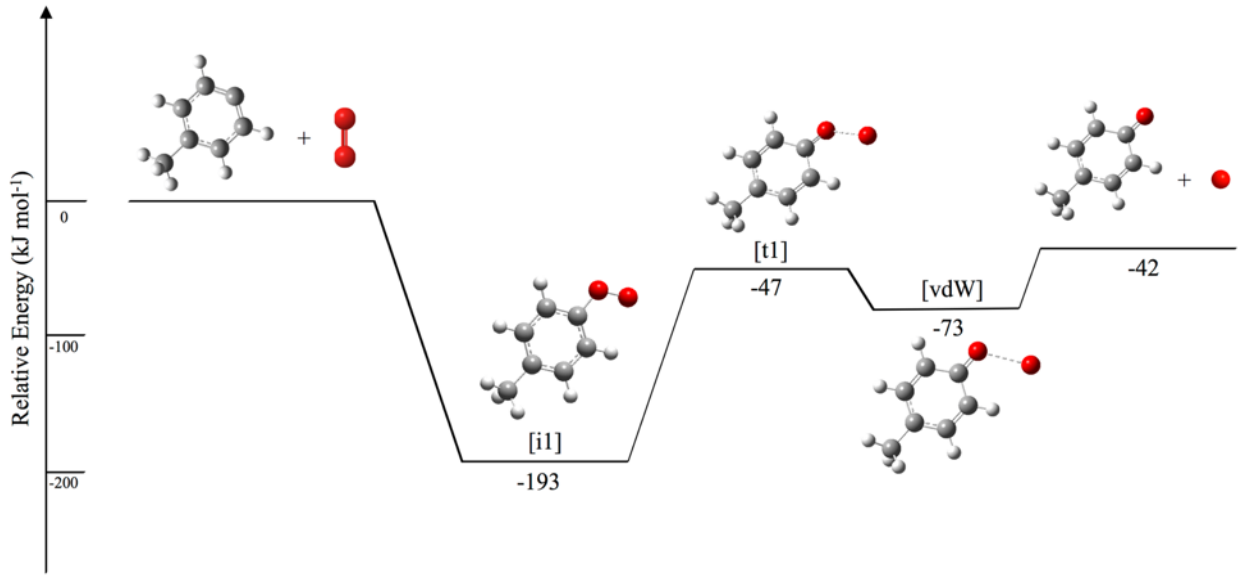

Figure 4. Potential energy diagram for the reaction of *p*-tolyl ($CH_3C_6H_4$, X^2A') with molecular oxygen (O_2, $X^3\Sigma_g^-$) forming the *p*-toloxy ($CH_3C_6H_4O$, X^2A') radical plus ground state atomic oxygen (O, ^3P_j) calculated at the G3(MP2,CC)//B3LYP/6-311++G** level of theory.